

TFFM: Topology-Aware Feature Fusion Module via Latent Graph Reasoning for Retinal Vessel Segmentation

Iftekhar Ahmed* Shakib Absar* Aftar Ahmad Sami† Shadman Sakib§
Debojyoti Biswas‡ Seraj Al Mahmud Mostafa§

*Leading University, Sylhet, Bangladesh, †University of Houston, Houston, TX, USA

§University of Maryland, Baltimore County, Baltimore, MD, USA

‡Pennsylvania State University, University Park, PA, USA

*{iftekharifat007, sabsar42}@gmail.com, †asami5@uh.edu

§{ssakib1, serajmostafa}@umbc.edu, ‡dbb5917@psu.edu

Abstract

Precise segmentation of retinal arteries and veins carries the diagnosis of systemic cardiovascular conditions. However, standard convolutional architectures often yield topologically disjointed segmentations, characterized by gaps and discontinuities that render reliable graph-based clinical analysis impossible despite high pixel-level accuracy. To address this, we introduce a topology-aware framework engineered to maintain vascular connectivity. Our architecture fuses a Topological Feature Fusion Module (TFFM) that maps local feature representations into a latent graph space, deploying Graph Attention Networks to capture global structural dependencies often missed by fixed receptive fields. Furthermore, we drive the learning process with a hybrid objective function, coupling Tversky loss for class imbalance with soft cIDice loss to explicitly penalize topological disconnects. Evaluation on the Fundus-AVSeg dataset reveals state-of-the-art performance, achieving a combined Dice score of 90.97% and a 95% Hausdorff Distance of 3.50 pixels. Notably, our method decreases vessel fragmentation by approximately 38% relative to baselines, yielding topologically coherent vascular trees viable for automated biomarker quantification. We open-source our code at <https://tffm-module.github.io/>.

1. Introduction

The human retina offers a unique, non-invasive window into the systemic microvasculature, where the geometric properties of arteries and veins (A/V) serve as potent biomarkers for cardiovascular disease, hypertension, and diabetic retinopathy. Currently, the standard of care relies on qualitative visual inspection or manual tracing, which is time-

consuming, subjective, and prone to inter-observer variability [10]. However, for these biomarkers to be clinically actionable, automated segmentation must yield more than just pixel-level accuracy; it must preserve the topological integrity of the vascular graph. To a clinician, a blood vessel is a continuous transport network; to a standard Convolutional Neural Network (CNN), it is merely a collection of disjoint pixels. This semantic gap is the primary cause of the shattered vessel phenomenon, where deep learning (DL) models achieve high Dice scores yet produce fragmented, topologically invalid segmentations that render graph-based analysis impossible.

In this work, we propose a topology-aware deep learning framework especially designed to address the dual challenges of class imbalance and structural continuity in A/V segmentation. Our approach is the result of a systematic ablation study identifying the optimal selection between architecture, encoder capacity, and loss formulation. In summary, we present a topology-aware framework that captures capillary regions. To overcome this, we introduce two key innovations. 1) **Topological Feature Fusion Module (TFFM):** We propose a novel module that projects feature maps into a latent graph space. By utilizing Graph Attention Networks (GATs) [26] within the decoder, the TFFM models the global connectivity of the vascular tree. It allows the network to reason about vessel continuity beyond the local receptive field of standard convolutions, and 2) **Hybrid Topology-Aware Objective:** We use a composite loss function combining Tversky loss [18], which addresses the foreground-background imbalance, with soft cIDice loss [21]. The latter acts as a topological regularizer, penalizing breaks in the vessel skeleton and ensuring the predicted morphology aligns with the curvilinear nature of the vasculature.

2. Related Works

Retinal vessel segmentation has evolved toward deep learning architectures, achieving high pixel-level accuracy, yet clinical utility depends on preserving vascular topology for biomarker extraction and graph-based analysis. Standard metrics (Dice, IoU) measure only region overlap, permitting topologically invalid segmentations where vessels fragment into disconnected components.

Multi-Scale Feature Architectures. Liu et al. [13] introduced IMFF-Net, achieving 0.9621 accuracy on DRIVE through Attention Pooling and multi-level feature fusion. However, optimizing solely with Dice loss yields no topology guarantees: high accuracy can mask severe fragmentation. Wang et al. [28] proposed Multi-Scale Attention Fusion to preserve spatial information during pooling. While capturing fine vessels, their local spatial attention cannot enforce global connectivity, resulting in broken bifurcations despite strong pixel metrics. Zhou et al. [34] combined dilated residuals with dual attention, but their hybrid loss remains topology-agnostic. These methods exemplify a critical limitation: architectural improvements for feature extraction do not translate to topological validity without explicit connectivity modeling.

State Space Models for Vessel Segmentation. Mamba-based architectures offer efficient long-range modeling. Wang et al. [29] proposed HM-Mamba with tubular structure-aware convolution, achieving 83.27% Dice on DRIVE. However, HM-Mamba lacks topology metrics, failing to distinguish continuous trees from fragmented predictions. Similarly, attention-enhanced Mamba [8] and TA-Mamba [20] improve feature modeling but lack graph-based reasoning about connectivity. Their evaluations emphasize sensitivity and specificity but omit skeleton-based metrics (clDice, junction detection) essential for structural fidelity. The fundamental issue persists: sequence modeling captures local dependencies but not global topological constraints.

Topology-Preserving Loss Functions. Shit et al. [21] introduced clDice loss, computing skeleton similarity to enforce connectivity. While pioneering topology-aware optimization, clDice alone sacrifices pixel accuracy and suffers from noise sensitivity. Zhang et al. [33] proposed clCE loss, improving robustness but remaining purely loss-based. Yeganeh et al. [32] developed SCOPE, encoding continuity as training constraints. These approaches share a critical weakness: applying topology constraints only during optimization, not feature extraction. The network architecture lacks components explicitly designed to model connectivity, limiting propagation of topological information through the feature hierarchy. Loss functions guide learning, but cannot compensate for architectures incapable of reasoning about vessel relationships.

Graph Neural Networks and Transformers. Li et

al. [12] proposed DE-DCGCN-EE with dynamic-channel graph convolution. However, their graphs operate on channel dimensions rather than spatial topology, missing geometric vessel relationships. Jalali et al. [9] developed VGA-Net with pixel-level graph nodes, but this design is prohibitively expensive at high resolutions. Wang et al. [27] combined transformers with adaptive upsampling (MICCAI 2022), while Tong et al. [25] introduced a lightweight LiViT-Net. Despite achieving high accuracy, transformer methods report no connectivity metrics and face quadratic complexity constraints at medical imaging resolutions. Taufik et al. [24] demonstrated transformers’ superiority for medical classification, yet their focus on interpretability leaves topology-preserving feature learning for segmentation unexplored.

Towards Architecture-Integrated Topology Preservation. Current methods optimize region overlap, often producing disconnected components despite high accuracy [13]. Such fragmentation renders predictions clinically unusable, as standard metrics (Dice, IoU) ignore topological relationships [15, 21]. A prediction achieving 95% Dice but containing 50 disconnected fragments scores identically to a topologically correct segmentation under standard metrics, despite being fundamentally incompatible with downstream clinical analysis. The absence of topology-specific metrics (clDice [21], Betti error, skeleton recall, junction detection) in most evaluations perpetuates this disconnect [15, 31]. To mitigate this issue, architectures can incorporate topological reasoning directly into feature extraction [11, 32, 33], enabling networks to learn representations that capture not only local vessel appearance but also the global connectivity constraints inherent to vascular trees.

In contrast to existing work, our method integrates topology preservation at both the architectural and loss levels through a TFFM with Graph Attention Networks and a hybrid Tversky + soft clDice objective that penalizes disconnections. This joint design produces topologically coherent vessel trees with substantially reduced fragmentation while preserving strong region-overlap performance suitable for downstream graph-based clinical analysis.

3. Methodology

In this work, we propose a topology-aware segmentation framework tailored for retinal artery–vein delineation (Fig. 1). The model builds upon a baseline identified through systematic ablation and is composed of a U-Net++ backbone enhanced with Attention Gates and an EfficientNet-B0 encoder. To preserve vascular connectivity, particularly in thin, tortuous structures, we introduce a Topological Feature Fusion Module (TFFM). TFFM explicitly captures and propagates topological cues across network levels. The training objective combines Tversky loss to mitigate class

Multi-Level TFFM Segmentation Architecture

Attention U-Net++ with TFFM Module

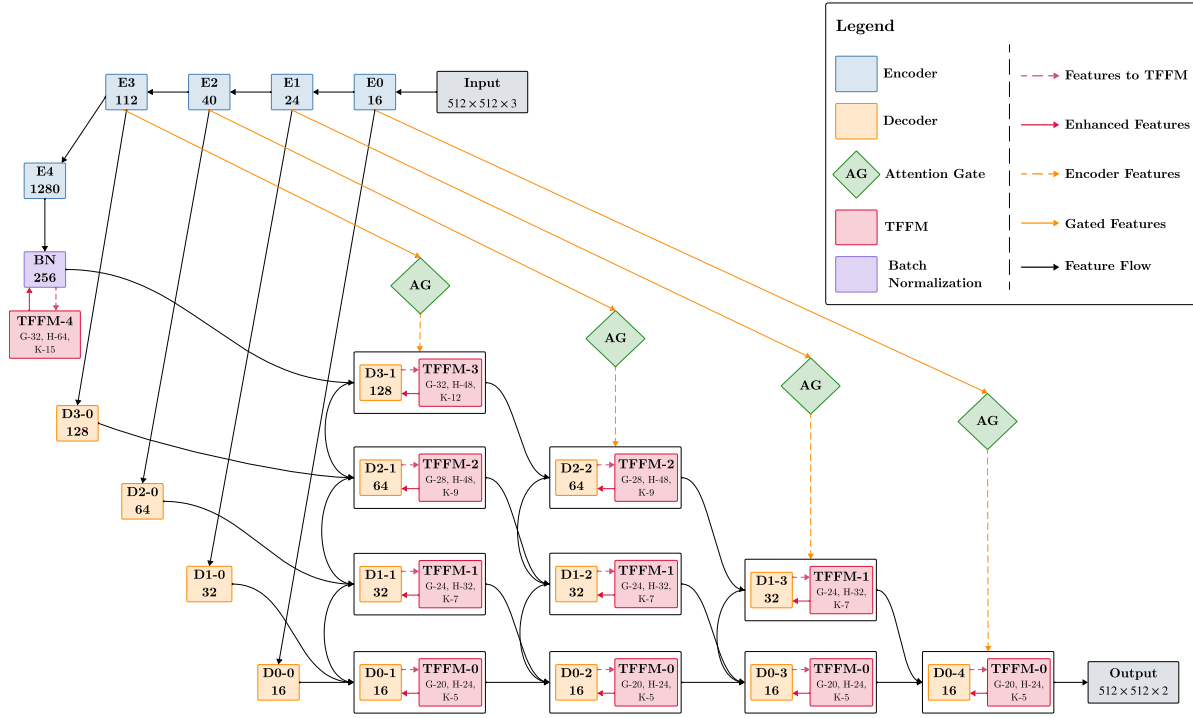


Figure 1. Overview of the proposed multi-level TFFM segmentation architecture.

imbalance with soft clDice loss to enforce structural continuity and reduce topological errors.

3.1. Baseline Architecture

The backbone architecture, established through comparative evaluation against U-Net [17], Attention U-Net [19], SegResNet [16], SwinUNETR [6], TransUNet [2], DeepLabV3+ [3], and Segformer [30], consists of U-Net++ [35] augmented with Attention Gates (AGs) [19].

It has been selected for its optimal performance in capturing fine-grained morphological details compared to standard U-Net and U-Net variants during our preliminary experimentation. The complete ablation study supporting this choice is presented in Section 5.1.

For the encoder path, we substitute standard convolutional blocks with an EfficientNet-B0 backbone [23]. Despite being a lighter model, EfficientNet-B0 achieved superior performance compared to the stronger EfficientNet-B4 variant in our experiments. This trend is affirmed by the full encoder ablation provided in Section 5.3.

3.2. Topological Feature Fusion Module (TFFM)

To address the inherent limitations in structural fidelity, we introduce the TFFM. While the backbone captures local features, TFFM projects these features into a latent graph space

to reason about global connectivity. The module (Figure 2) operates in four stages: multi-scale abstraction, dynamic graph reasoning, attention-based refinement, and adaptive integration.

Scale-Adaptive Abstraction and Graph Construction:

The TFFM is applied at each decoder level l with depth-dependent hyperparameters: grid size G_l , hidden dimension $C_{h,l}$, and neighbor count k_l . The input \mathbf{X} is first compressed to $C_{h,l}$ channels using a 1×1 convolution. Two pooled representations are then generated: a primary grid $\mathbf{F}_{main} \in \mathbb{R}^{C_{h,l} \times G_l \times G_l}$ and an auxiliary grid \mathbf{F}_{aux} of size $\max(G_l/2, 4)$. This ensures a minimum coarse resolution.

We form a feature-space graph $\mathcal{G} = (\mathcal{V}, \mathcal{E})$ where nodes are vectors in the flattened \mathbf{F}_{main} . A cosine similarity matrix \mathbf{S} is computed and sparsified via top- k_l selection:

$$\mathbf{A}_{ij} = \mathbb{I}(j \in \text{top-}k_l(\mathbf{S}_{i:})), \quad \tilde{\mathbf{A}} = \mathbf{A} + \mathbf{I}, \quad (1)$$

Graph Attention: We utilize a Graph Attention Network (GAT) [26] with masked attention. The unnormalized attention scores are computed and masked by the adjacency structure:

$$e_{ij} = \text{LeakyReLU}(\mathbf{a}^T [\mathbf{W}\mathbf{h}_i \parallel \mathbf{W}\mathbf{h}_j]) \cdot \tilde{\mathbf{A}}_{ij}, \quad (2)$$

$$\alpha_{ij} = \text{softmax}_j(e_{ij}/\tau), \quad (3)$$

TFFM: Topological Feature Fusion Module

Feature-based Graph + GAT Reasoning

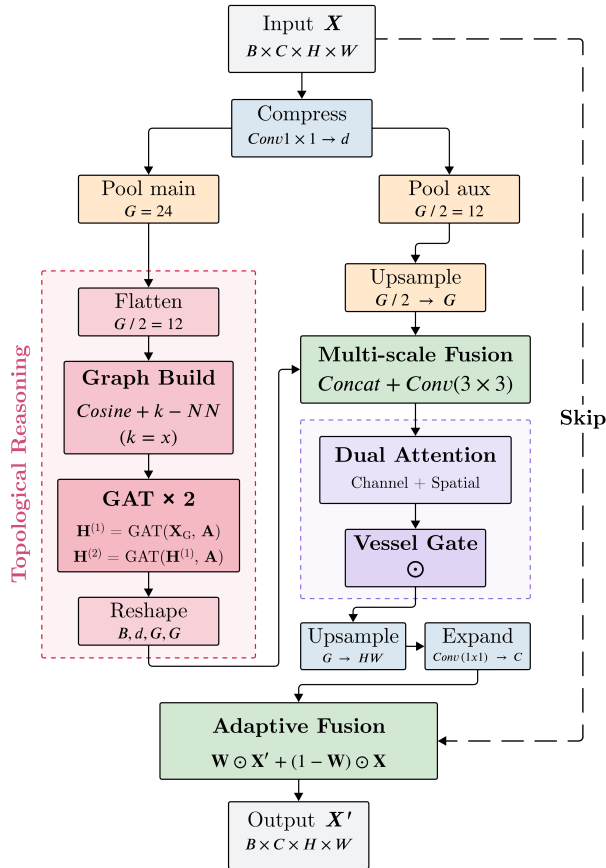


Figure 2. Overview of the proposed TFFM

where τ is a learnable temperature parameter. Non-neighbors (where $\tilde{\mathbf{A}}_{ij} = 0$) contribute zero to the attention logits, effectively being pruned from the aggregation.

Multi-scale Fusion and Refinement: The output graph features are reshaped to $\mathbb{R}^{C_{h,l} \times G_l \times G_l}$ and concatenated with the upsampled auxiliary features. A 3×3 convolution produces the fused representation \mathbf{F}_{fused} . Channel Attention Module (CAM) and Spatial Attention Module (SAM) refine this tensor:

$$\mathbf{F}_{att} = \mathbf{F}_{fused} \odot \text{CAM}(\mathbf{F}_{fused}) \odot \text{SAM}(\mathbf{F}_{fused}), \quad (4)$$

followed by a vesselness gating mechanism where \mathcal{F}_{vessel} is a lightweight CNN that predicts vessel-relevant weights:

$$\mathbf{F}_{ref} = \mathbf{F}_{att} \odot \sigma(\mathcal{F}_{vessel}(\mathbf{F}_{att})), \quad (5)$$

Adaptive Integration: The refined features are upsampled to (H, W) and expanded back to the original chan-

nel dimension. A learnable gated residual connection then blends local and topological information:

$$\lambda = \sigma(\Psi_{gate}([\mathbf{X} \parallel \mathbf{F}_{exp}])), \quad (6)$$

$$\mathbf{Y} = \lambda \odot \Psi_{fusion}([\mathbf{X} \parallel \mathbf{F}_{exp}]) + (1 - \lambda) \odot \mathbf{X}, \quad (7)$$

This gate allows the network to selectively inject global connectivity cues while preserving fine local structure.

3.3. Loss Function

To address retinal artery/vein segmentation, we employ a hybrid loss function combining Tversky Loss (L_{Tv}) for handling the extreme foreground-background class imbalance and soft cIDice Loss (L_{clDice}) for preserving topological connectivity of thin vessels. The total loss is averaged over both vessel classes.

Tversky Loss: We employ Tversky loss to mitigate foreground-background imbalance by asymmetrically weighting false positives and negatives. For predictions P_c and ground truth G_c , we define the true positives $TP = \sum p_{ci}g_{ci}$, false negatives $FN = \sum(1 - p_{ci})g_{ci}$, and false positives $FP = \sum p_{ci}(1 - g_{ci})$. The Tversky index is formulated as:

$$TI(P_c, G_c) = \frac{TP}{TP + \alpha FN + \beta FP}, \quad (8)$$

In our experiments, we observed that missed vessel segments (false negatives) break the vascular topology more severely than background noise (false positives). Consequently, we tune the hyperparameters to prioritize recall. We set $\alpha = 0.65$ to increase the penalty for false negatives. Following the standard implementation in the MONAI framework, β is set to $1 - \alpha = 0.35$. The Tversky loss is then computed as:

$$L_{Tv} = 1 - \frac{1}{C} \sum_{c=1}^C TI(P_c, G_c), \quad (9)$$

Soft cIDice Loss: While L_{Tv} improves pixel-level accuracy, it does not explicitly penalize topological breaks. We therefore incorporate the soft cIDice loss, which operates on the continuous probability maps to preserve connectivity. We apply a differentiable *soft-skeletonization* function $S(\cdot)$ to both the predicted probabilities P and the ground truth G . This algorithm uses iterative min/max-pooling operations to approximate the morphological skeleton on soft inputs:

$$\begin{aligned} S(P) &= \text{SoftSkeletonize}(P), \\ S(G) &= \text{SoftSkeletonize}(G), \end{aligned} \quad (10)$$

Using these soft skeletons, we compute the Topological Precision (T_{prec}) and Topological Sensitivity (T_{sens}),

which measure the overlap between the predicted soft skeleton and the ground truth mask (and vice-versa):

$$T_{prec}(S(P), G) = \frac{|S(P) \cap G|}{|S(P)|},$$

$$T_{sens}(S(G), P) = \frac{|S(G) \cap P|}{|S(G)|}, \quad (11)$$

The clDice index is the harmonic mean of these measures. The loss is minimized to ensure the network preserves the graph-like structure of the vasculature:

$$L_{clDice} = 1 - \frac{2 T_{prec} T_{sens}}{T_{prec} + T_{sens}}, \quad (12)$$

Composite Objective: The final objective function L_{total} is a weighted sum of the region-based Tversky loss and the topology-aware clDice loss:

$$L_{total} = L_{Tv} + \lambda L_{clDice}, \quad (13)$$

Based on our empirical evaluations, we set the weighting factor $\lambda = 0.5$. This configuration balances volumetric segmentation accuracy with the preservation of vascular connectivity across both artery and vein channels.

4. Experiments

4.1. Dataset

We use the **Fundus-AVSeg** dataset [4], a recent benchmark for artery–vein segmentation containing 100 high-resolution fundus images (2656×1992 or 1280×1280) captured with ZEISS VISUCAM200 and Canon cameras at Shenzhen Eye Hospital. Annotations were produced through a multi-stage protocol involving six junior and one senior ophthalmologist, providing pixel-level labels for arteries, veins, crossings, and uncertain vessels.

4.2. Implementation Details

Data Pre-processing and Augmentation: The dataset was randomly partitioned into training (80%), validation (10%), and testing (10%) subsets. To ensure experimental reproducibility, a fixed random seed was utilized for the split. All input images and corresponding masks were resized to a spatial resolution of 512×512 pixels. Intensity scaling was applied to the images to normalize the pixel value range. We implemented a comprehensive online data augmentation pipeline using the MONAI library. Table 1 shows the details of the augmentation strategies applied during the training phase.

TFFM Configuration: To effectively inject global structural awareness into the local receptive fields, we implemented the TFFM with scale-adaptive hyperparameters. As direct graph construction on 512^2 pixels is computationally prohibitive, we utilized the module’s adaptive pooling

Augmentation Technique	Parameters	Probability
Random Rotation	Range $\in [-30^\circ, +30^\circ]$	0.5
Vertical Flip	-	0.5
Horizontal Flip	-	0.5
Affine Translation	Shift limit = 5%	0.3
Random Contrast	$\gamma \in [0.8, 1.2]$	0.3
Intensity Shift	Offset = 0.1	0.3
Gaussian Noise	$\mu = 0, \sigma = 0.01$	0.2
Gaussian Smoothing	$\sigma \in [0.5, 1.0]$	0.2

Table 1. Data augmentation techniques with hyperparameters.

to transform feature maps into manageable coarse grids, thereby shifting the paradigm from spatial proximity to content-based similarity. The TFFM was applied at decoder levels $l \in \{0, 1, 2, 3, 4\}$ to resolve the tunnel vision limitation of standard convolutions. The grid sizes (G_l) were configured progressively as $\{20, 24, 28, 32, 32\}$, with corresponding neighbor counts (k_l) of $\{5, 7, 9, 12, 15\}$. This configuration ensures that deeper levels (with higher k) capture broader global dependencies to maintain vessel continuity, while shallower levels preserve local feature fidelity.

Training Setup: The proposed framework was implemented in PyTorch and MONAI. All experiments were conducted on an NVIDIA H200 GPU. The model was optimized using the AdamW optimizer with an initial learning rate of 1×10^{-3} . We utilized a batch size of 10. The training process was set to run for a maximum of 500 epochs, incorporating an early stopping mechanism with a patience of 10 epochs. Training was halted if the validation loss did not improve within this window.

Experimental Progression: To isolate the contribution of each architectural component, we followed a systematic ablation strategy where only one variable was modified at a time. The overall workflow is illustrated in Figure 3 and detailed below:

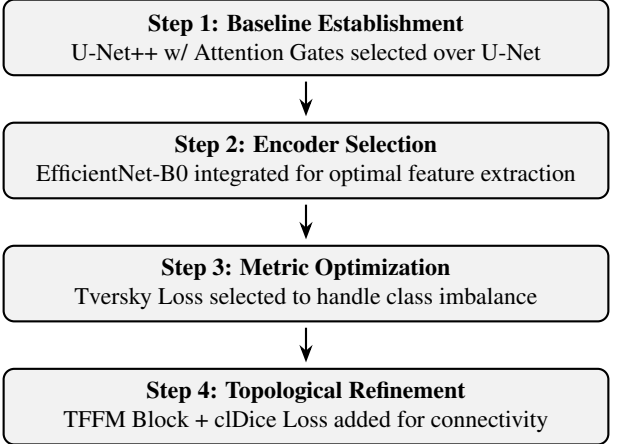


Figure 3. Systematic experimental progression used to derive the final topology-aware framework.

4.3. Evaluation Metrics

To fully assess the performance of our model, we employ two categories of metrics: pixel-wise segmentation metrics and topology-aware structural metrics.

Pixel-wise Metrics: We report the Dice Similarity Coefficient (DSC) and Intersection over Union (IoU) to measure region overlap. To evaluate boundary accuracy, which is critical for thin vessels, we compute the 95% Hausdorff Distance (HD95). HD95 is computed separately for arteries and veins against their respective ground truth, and on merged masks for combined vessel segmentation.

Topological and Connectivity Metrics: Standard pixel metrics often fail to penalize broken vessel connections. Therefore, we include:

- **cIDice** [21]: A topology-preserving metric that calculates the harmonic mean of topological precision and sensitivity based on the vascular skeleton.
- **Betti Number Error (Betti0-Err):** This metric measures the difference in the number of connected components between prediction and ground truth. A lower error indicates better preservation of vascular connectivity, with fewer fragmented vessel segments.
- **Skeleton-F1 and Junction-Recall:** We skeletonize the prediction and ground truth to measure the F1-score of the vessel centerlines and the recall rate of bifurcation points (junctions), which are essential for graph-based downstream analysis.

5. Results

To establish a robust framework for topology-aware vessel segmentation, we adopted a systematic ablation strategy. We optimize the pipeline sequentially shown in Section 4.2.

5.1. Baseline Architecture Selection

We first evaluated segmentation architectures under controlled conditions (BCE loss, AdamW, no augmentation, no pre-trained encoder). Table 2 presents the performance on the combined vasculature.

Architecture	IoU(%)	Dice(%)	HD95	Precision(%)	Recall(%)
U-Net	62.86	77.10	12.45	94.11	65.67
Attention U-Net	81.45	89.75	4.60	93.40	86.55
U-Net++	81.69	89.89	4.27	95.19	85.36
U-Net++ w/ Attn	83.52	91.00	3.59	94.05	88.31
SegResNet	79.08	88.29	7.05	94.05	83.36
TransUNet (ViT-B)	73.29	84.56	8.34	90.19	79.75
SwinUNETR	74.76	85.54	9.97	95.04	77.94
DeepLabV3+	49.02	65.76	11.00	73.28	59.77
Segformer	66.00	79.48	7.78	85.19	74.72

Table 2. Baseline architectural comparison (combined).

As Unet++ and Attention U-Net performed well, we integrated U-Net++ with Attention Gates, which achieved the highest Dice (91%) and lowest boundary error (HD95: 3.59). The nested skip connections preserved multi-scale

features, while Attention Gates successfully improved recall to 88.31% without sacrificing precision (94.05%). Transformer-based models (TransUNet, SwinUNETR) underperformed in this data-constrained regime compared to the nested convolutional approach.

5.2. Baseline Loss Function Optimization

To identify a loss function suitable for both class imbalance and topological continuity, we evaluated BCEDice, BoundaryDoU, LogCoshDice, and Tversky Loss ($\alpha = 0.65$) using a fixed U-Net++ with Attention Gates architecture.

A qualitative summary of strengths and weaknesses is provided in Table 3. Quantitatively, LogCoshDice achieved the highest scores in pixel-level accuracy (Dice: 92.04%, HD95: 2.98) and centerline metrics (Cent-Dice: 75.49%). Conversely, BoundaryDoU excelled in topological continuity, recording the lowest Betti0 error (25.5) and the least fragmentation (27.2 components, avg. length 310.20). The Tversky loss provided a robust balance between these two profiles, consistently achieving the second-best result in nearly every category, including topology (Betti0 error: 27.3), fragmentation, and centerline accuracy without placing first in pixel metrics. Given that vessel segmentation prioritizes topological fidelity, Tversky loss was selected as the optimal baseline for subsequent experiments.

Loss	Strengths	Weaknesses
BCEDice	Simple baseline with reasonable recall	Highest fragmentation and weak topology
BoundaryDoU	Lowest topological error and minimal fragmentation	Blurred boundaries and reduced connectivity
LogCoshDice	Best pixel metrics and highest Skel-F1	Higher topological error and moderate fragmentation
Tversky ($\alpha = 0.65$)	Balanced topology, connectivity, and boundary accuracy	Slightly below LogCoshDice in pixel metrics

Table 3. Qualitative comparison of the evaluated loss functions.

5.3. Encoder Selection

We evaluated five pretrained encoders integrated within the U-Net++ (Attn) + Tversky pipeline. Table 4 presents the comparative performance across key metrics.

EfficientNet-B0 delivered the best individual vessel performance, achieving the highest Dice scores for both artery (81.80%) and vein (84.32%) while substantially improving boundary accuracy (HD95: 25.08/19.05). Notably, it outperformed the larger EfficientNet-B4 despite using 75% fewer parameters, suggesting superior model-dataset fit. While ResNet-101 achieved marginally higher combined-class Dice (90.63%), it exhibited greater fragmentation in

Encoder	Metric	Artery	Vein	Combined
EffNet-B0	Dice (%) \uparrow	81.80	84.32	90.15
	HD95 \downarrow	25.08	19.05	
	Betti0-Err \downarrow	38.60	38.00	
ResNet-101	Dice (%) \uparrow	80.98	84.05	90.63
	HD95 \downarrow	27.88	20.83	
	Betti0-Err \downarrow	44.40	34.80	
ConvNeXt-B	Dice (%) \uparrow	80.96	83.98	90.24
	HD95 \downarrow	28.34	20.67	
	Betti0-Err \downarrow	48.10	44.40	
EffNet-B4	Dice (%) \uparrow	79.11	82.14	90.27
	HD95 \downarrow	26.94	23.00	
	Betti0-Err \downarrow	38.40	46.40	
ResNet-50	Dice (%) \uparrow	80.56	83.44	89.89
	HD95 \downarrow	27.33	19.67	
	Betti0-Err \downarrow	51.60	36.10	

Table 4. Encoder comparison (U-Net++ Attn + Tversky).

arteries (Betti0-Error: 44.40 vs 38.60) and inferior sensitivity to fine vessel details. EfficientNet-B0’s balance of per-class accuracy, minimal topological fragmentation, and computational efficiency established it as the optimal encoder.

5.4. Topological Refinement (TFFM)

Having fixed the backbone (U-Net++ w/ Attn), loss (Tversky), and encoder (EfficientNet-B0), we introduced the proposed TFFM.

Configuration	Comb. Dice(%)	clDice(%)	Betti0-Err	Junc-F1(%)
EffNet-B0 (Baseline)	90.15	84.54	43.0	63.64
Baseline + TFFM	90.47	85.05	26.0	65.44

Table 5. Impact of TFFM on topology.

As shown in Table 5, TFFM integration improved topological fidelity: Betti number error dropped by 39.5% (43.0 \rightarrow 26.0), and junction detection F1-score increased from 63.64% to 65.44%. These gains were accompanied by modest improvements in per-class segmentation (Artery Dice: 81.80% \rightarrow 82.39%, Vein Dice: 84.32% \rightarrow 84.77%) and reduced Hausdorff distances. The module also reduced over-fragmentation: predicted components decreased from 44.7 to 27.7 (38% reduction), aligning better with the ground truth topology.

5.5. Final Model: Topological Loss and Augmentation

To maximize generalization and connectivity, we incorporated the soft clDice loss ($L_{total} = L_{Tv} + 0.5L_{clDice}$) into the TFFM framework and applied a comprehensive augmentation pipeline (realistic rotations, flips, translation, brightness/contrast adjustments, Gaussian noise/blur). This

final configuration achieved a validation Dice of 87.20% at epoch 72, substantially improving generalization over the non-augmented TFFM model (83.31%).

Metric	Artery	Vein	Combined
Dice Score(%) \uparrow	85.75	87.63	90.97
HD95 (px) \downarrow	21.22	14.59	3.50
clDice(%) \uparrow	79.07	81.46	85.55
Pred. Components \downarrow	23.3	26.1	25.3

Table 6. Final proposed framework performance.

The final model delivered improvements across all metrics (Table 6). Artery and vein Dice scores increased to 85.75% and 87.63%, respectively, while HD95 distances decreased to 21.22 and 14.59, enhancing boundary accuracy for thin vessels. The clDice metric improved substantially to 85.55%, with skeleton F1 scores reaching 87.63% for arteries and 88.48% for veins. Most critically, fragmentation was minimized to 25.3 predicted components, the lowest achieved, yielding highly continuous vessel trees. Junction detection precision improved to 0.63/0.71 for artery/vein, though recall remains limited at 0.44/0.52, suggesting future work should focus on branch point completeness. These results confirm that the framework produces topologically robust segmentations suitable for automated graph analysis.

6. Cross-Dataset Generalization and Transferability Analysis

To rigorously evaluate the generalization capability of our proposed TFFM architecture, we conducted an extensive cross-dataset validation study. Unlike conventional within-dataset evaluations, we performed zero-shot inference on five established retinal vessel segmentation benchmarks without any fine-tuning or adaptation. This protocol assesses the model’s robustness to variations in imaging protocols, scanner types, and pathological presentations.

6.1. Experimental Protocol

The model trained on Fundus-AVSeg (Section 4.1) was directly applied to external test sets. All images were pre-processed identically, resized to 512 \times 512 pixels, and intensity-normalized. No augmentation was applied during inference. We report comprehensive metrics that span pixel-wise accuracy, topological fidelity, and junction detection to provide a holistic assessment of domain adaptation.

6.2. Cross-Dataset Quantitative Performance

Table 7 presents the aggregated performance metrics across five publicly available datasets representing diverse imaging conditions. Our framework maintained strong segmentation quality and, notably, preserved topological consistency.

Dataset	Dice(%) \uparrow	HD95 \downarrow	clDice(%) \uparrow	Betti0-Err \downarrow	Junc-F1(%) \uparrow
DRIVE [22]	82.10	10.20	70.67	24.20	30.63
CHASEDB1 [5]	80.61	12.77	68.71	50.50	41.42
HRF [1]	79.94	12.67	73.01	33.00	55.10
RETA [14]	82.18	15.31	73.57	34.57	51.34
STARE [7]	80.70	33.25	70.98	41.55	43.34

Table 7. Cross-dataset inference performance (combined vasculature).

Vessel Segmentation Accuracy: The model achieved Dice coefficients ranging from 79.94% (HRF) to 82.18% (RETA), showing robust pixel-level performance across domains. Notably, DRIVE and RETA results approached the performance on the source domain (Fundus-AVSeg: 82.18% vs. 90.97%), indicating strong alignment with healthy retinal morphology. The elevated HD95 on STARE (33.25 px) and RETA (15.31 px) reflects challenges with pathological cases and high myopia, where vessel caliber and tortuosity differ significantly from training data.

Topological Consistency: The clDice metric remained consistently high (68.71%–73.57%), substantially outperforming traditional methods in zero-shot settings. The lowest Betti0-Error on DRIVE (24.20) confirms superior preservation of vascular connectivity for standard screening images. However, CHASEDB1 exhibited higher fragmentation (Betti0-Error: 50.50), likely due to pediatric vasculature patterns unseen during training. Despite this, skeleton F1-scores remained strong (82.68%–87.41%), indicating that predicted centerlines remained spatially aligned even when minor breaks occurred.

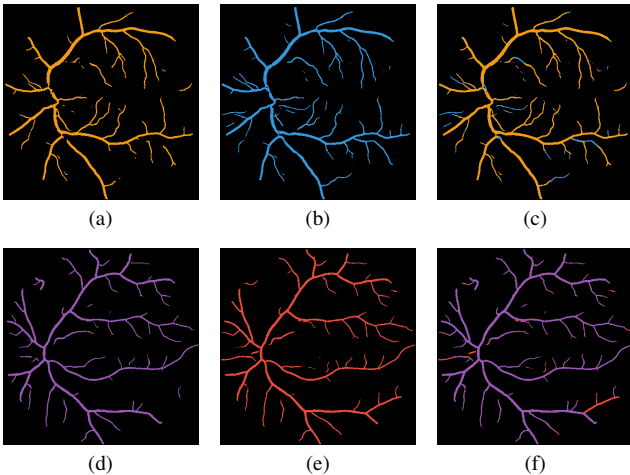


Figure 4. Vein and Artery prediction visualization comparing performance with and without TFFM. Top row: (a) vein prediction without TFFM, (b) vein prediction with TFFM, (c) vein overlay. Bottom row: (d) artery prediction without TFFM, (e) artery prediction with TFFM, (f) artery overlay.

7. Discussions

Our results highlight the critical disconnect between pixel-level accuracy and topological validity in retinal vessel seg-

mentation. Baseline methods like LogCoshDice achieved high Dice scores (92.04%) but failed to maintain structural integrity, with high topological error (Betti0-Err: 30.7), corroborating the intrinsic topological vulnerability of standard CNNs that yield disjointed predictions clinically unusable for graph-based analysis. Integration of our TFFM resolved this disparity by mapping local features into a latent graph space, enabling the network to reason about global connectivity and reducing fragmented components by 38% (from 44.7 to 27.7) even before full augmentation, as visualized in Figure 4.

The ablation study validated our architectural choices: EfficientNet-B0 outperformed deeper encoders like ResNet-101, suggesting parameter-efficient networks better preserve fine spatial details for thin vessel segmentation. The relationship between Tversky loss (prioritizing recall) and soft clDice loss (penalizing topological breaks) was essential. TFFM integration alone reduced Betti error by 39.5%, a gain unachievable by pixel-based losses. Crucially, this structural fidelity extends to zero-shot inference on external datasets, confirming that the learned topological constraints are robust to variations in scanner protocols and not merely overfitted to the training distribution. However, bifurcation completeness remains limited, with junction recall at 0.44 for arteries and 0.52 for veins, indicating the network still struggles with extreme local complexity at crossing points despite preserving global vessel tree connectivity, necessitating future specialized attention mechanisms. Clinically, these topological failures in complex bifurcations pose a risk for automated tortuosity quantification, which requires expert review for pathological cases. Future deployment on standard clinical workstations will require further validation to ensure these automated topological metrics correlate robustly with patient outcomes across diverse populations.

8. Conclusions

We introduced a topology-aware framework for retinal artery-vein segmentation that addresses vascular fragmentation by integrating TFFM with a hybrid objective function to capture global connectivity while maintaining local features. On the Fundus-AVSeg dataset, our method achieves state-of-the-art performance with 90.97% combined Dice score, 3.50 pixels HD95, and critically reduces fragmentation to 25.3 components per image, significantly outperforming baselines. These results confirm our framework generates topologically robust segmentations advantageous for automated biomarker extraction. Limited junction recall suggests bifurcation-aware attention mechanisms could improve branch point completeness. Future work includes extending to pathological datasets, lightweight variants for clinical deployment, and end-to-end graph architectures for arteriovenous classification and tortuosity quantification.

References

[1] A. Budai, R. Bock, A. Maier, J. Hornegger, and G. Michelson. Robust vessel segmentation in fundus images. *International Journal of Biomedical Imaging*, 2013(1):154860, 2013. 8

[2] Jieneng Chen, Jieru Mei, Xianhang Li, Yongyi Lu, Qihang Yu, Qingyue Wei, Xiangde Luo, Yutong Xie, Ehsan Adeli, Yan Wang, et al. Transunet: Rethinking the u-net architecture design for medical image segmentation through the lens of transformers. *Medical Image Analysis*, 97:103280, 2024. 3

[3] Liang-Chieh Chen, Yukun Zhu, George Papandreou, Florian Schroff, and Hartwig Adam. Encoder-decoder with atrous separable convolution for semantic image segmentation. In *Proceedings of the European conference on computer vision (ECCV)*, pages 801–818, 2018. 3

[4] Zhuo Deng, Weihao Gao, Zheng Gong, Run Gan, Lu Chen, Shaochong Zhang, and Lan Ma. A fundus image dataset for AI-based artery-vein vessel segmentation. *Scientific Data*, 12:1298, 2025. 5

[5] Muhammad Moazam Fraz, Paolo Remagnino, Andreas Hoppe, Bunyarat Uyyanonvara, Alicja R. Rudnicka, Christopher G. Owen, and Sarah A. Barman. Chase db1: Retinal vessel reference dataset, 2012. 8

[6] Ali Hatamizadeh, Vishwesh Nath, Yucheng Tang, Dong Yang, Holger R Roth, and Daguang Xu. Swin unetr: Swin transformers for semantic segmentation of brain tumors in mri images. In *International MICCAI brainlesion workshop*, pages 272–284. Springer, 2021. 3

[7] A. Hoover, V. Kouznetsova, and M. Goldbaum. Stare: Structured analysis of the retina dataset, 2000. 8

[8] Hang Hu, Haoren Xiong, Fei Long, Mohammad S. Alam, and Jun Sang. Multi-scale vision mamba-unet: A mamba-based method for retinal vessel segmentation. *Biomedical Signal Processing and Control*, 2025. 2

[9] Yeganeh Jalali, Mansoor Fateh, and Mohsen Rezvani. VGA-Net: Vessel graph based attentional U-Net for retinal vessel segmentation. *IET Image Processing*, 18(8):2191–2213, 2024. 2

[10] Ali Khandouzi, Ali Ariaifar, Zahra Mashayekhpour, Milad Pazira, and Yasser Baleghi. Retinal vessel segmentation, a review of classic and deep methods. *Annals of Biomedical Engineering*, 50(10):1292–1314, 2022. 1

[11] Liangzhi Li, Manisha Verma, Yuta Nakashima, Hajime Nagahara, and Ryo Kawasaki. Iternet: Retinal image segmentation utilizing structural redundancy in vessel networks. In *IEEE Winter Conference on Applications of Computer Vision (WACV)*, pages 3645–3654, 2020. 2

[12] Yang Li, Yue Zhang, Weigang Cui, Baiying Lei, Xihe Kuang, and Teng Zhang. Dual encoder-based dynamic-channel graph convolutional network with edge enhancement for retinal vessel segmentation. *IEEE Transactions on Medical Imaging*, 41(8):1975–1989, 2022. 2

[13] Mingzhe Liu, Yunyu Wang, Lei Wang, Shaoyi Hu, Xin Wang, and Qingli Ge. Imff-net: An integrated multi-scale feature fusion network for accurate retinal vessel segmenta-
tion from fundus images. *Biomedical Signal Processing and Control*, 91:105980, 2024. 2

[14] X. Lyu, L. Cheng, and S. Zhang. Reta: A retinal dataset. *Scientific Data*, 9, 2022. 8

[15] Agata Mosinska, Pablo Marquez-Neila, Mateusz Kozinski, and Pascal Fua. Beyond the pixel-wise loss for topology-aware delineation. In *2018 IEEE/CVF Conference on Computer Vision and Pattern Recognition*, pages 3136–3145, 2018. 2

[16] Andriy Myronenko. 3d mri brain tumor segmentation using autoencoder regularization. In *International MICCAI brainlesion workshop*, pages 311–320. Springer, 2018. 3

[17] Olaf Ronneberger, Philipp Fischer, and Thomas Brox. U-net: Convolutional networks for biomedical image segmentation. In *International Conference on Medical image computing and computer-assisted intervention*, pages 234–241. Springer, 2015. 3

[18] Seyed Sadegh Mohseni Salehi, Deniz Erdogmus, and Ali Gholipour. Tversky loss function for image segmentation using 3d fully convolutional deep networks. In *International workshop on machine learning in medical imaging*, pages 379–387. Springer, 2017. 1

[19] Jo Schlemper, Ozan Oktay, Michiel Schaap, Mattias Heinrich, Bernhard Kainz, Ben Glocker, and Daniel Rueckert. Attention gated networks: Learning to leverage salient regions in medical images. *Medical image analysis*, 53:197–207, 2019. 3

[20] Dangguo Shao, Rui Xu, Lei Ma, and Sanli Yi. Tubular-aware mamba for accurate retinal vessel segmentation: preserving fine details and topological connectivity. *Multimedia Systems*, 31, 2025. 2

[21] Suprosanna Shit, Johannes C. Paetzold, Anjany Sekuboyina, Ivan Ezhov, Alexander Unger, Andrey Zhylka, Josien P. W. Pluim, Ulrich Bauer, and Bjoern H. Menze. cldice—a novel topology-preserving loss function for tubular structure segmentation. In *Proceedings of the IEEE/CVF Conference on Computer Vision and Pattern Recognition*, pages 16560–16569, 2021. 1, 2, 6

[22] J. Staal, M.D. Abràmoff, M. Niemeijer, M.A. Viergever, and B. van Ginneken. Ridge-based vessel segmentation in color images of the retina. *IEEE Transactions on Medical Imaging*, 23(4):501–509, 2004. 8

[23] Mingxing Tan and Quoc Le. Efficientnet: Rethinking model scaling for convolutional neural networks. In *International conference on machine learning*, pages 6105–6114. PMLR, 2019. 3

[24] Enam Ahmed Taufik, Abdullah Khondoker, Antara Firoz Parsa, and Seraj Al Mahmud Mostafa. Visual bias and interpretability in deep learning for dermatological image analysis. In *2025 4th International Conference on Image Processing and Media Computing (ICIPMC)*, pages 45–49. IEEE, 2025. 2

[25] Le Tong, Tianjiu Li, Qian Zhang, Qin Zhang, Renchaoli Zhu, Wei Du, and Pengwei Hu. Livit-net: A u-net-like, lightweight transformer network for retinal vessel segmentation. *Computational and Structural Biotechnology Journal*, 24:213–224, 2024. 2

- [26] Petar Veličković, Guillem Cucurull, Arantxa Casanova, Adriana Romero, Pietro Liò, and Yoshua Bengio. Graph Attention Networks. *International Conference on Learning Representations*, 2018. accepted as poster. [1](#), [3](#)
- [27] Changwei Wang, Rongtao Xu, Shibiao Xu, Weiliang Meng, and Xiaopeng Zhang. Da-net: Dual branch transformer and adaptive strip upsampling for retinal vessels segmentation. In *Medical Image Computing and Computer Assisted Intervention – MICCAI 2022*, pages 528–538, Cham, 2022. Springer Nature Switzerland. [2](#)
- [28] Shubin Wang, Yuanyuan Chen, and Zhang Yi. A multi-scale attention fusion network for retinal vessel segmentation. *Applied Sciences*, 14(7):2955, 2024. [2](#)
- [29] Tao Wang, Dongyuan Tian, Haonan Zhao, Jiamin Liu, Weijie Wang, Chunpei Li, and Guixia Liu. Hierarchical multi-scale mamba with tubular structure-aware convolution for retinal vessel segmentation. *Entropy*, 27(8):862, 2025. [2](#)
- [30] Enze Xie, Wenhui Wang, Zhiding Yu, Anima Anandkumar, Jose M Alvarez, and Ping Luo. Segformer: Simple and efficient design for semantic segmentation with transformers. *Advances in neural information processing systems*, 34: 12077–12090, 2021. [3](#)
- [31] Ziyun Yang and Sina Farsiu. Directional connectivity-based segmentation of medical images. In *Proceedings of the IEEE/CVF Conference on Computer Vision and Pattern Recognition (CVPR)*, pages 11525–11535, 2023. [2](#)
- [32] Yasaman Yeganeh, Gökhan Güvercin, Rui Xiao, Matthew Garratt, Johannes C Paetzold, Suprosanna Shit, and Ali Ertuğrul Gözü. Scope: Structural continuity preservation for retinal vessel segmentation. In *International Workshop on Graphs in Biomedical Image Analysis*, pages 3–13. Springer, 2023. [2](#)
- [33] Zhiyuan Zhang, Ruisheng Liu, Qiming Ma, Yingfeng Xia, Yongpeng Lu, and Danny Z Chen. The centerline-cross entropy loss for vessel-like structure segmentation: Better topology consistency without sacrificing accuracy. In *International Conference on Medical Image Computing and Computer-Assisted Intervention*, pages 770–780. Springer, 2024. [2](#)
- [34] Jinzhi Zhou, Guangcen Ma, Haoyang He, Saifeng Li, and Guopeng Zhang. A multi-scale feature extraction and fusion-based model for retinal vessel segmentation in fundus images. *Medical & Biological Engineering & Computing*, 63(2):595–608, 2024. [2](#)
- [35] Zongwei Zhou, Md Mahfuzur Rahman Siddiquee, Nima Tajbakhsh, and Jianming Liang. Unet++: A nested u-net architecture for medical image segmentation. In *International workshop on deep learning in medical image analysis*, pages 3–11. Springer, 2018. [3](#)